Rapid Aero Modeling for Urban Air Mobility Aircraft in Wind-Tunnel Tests

Patrick C. Murphy,[1] Benjamin M. Simmons,[2] David B. Hatke,[3] and Ronald C. Busan[4]
NASA Langley Research Center, Hampton, VA, 23681

Rapid Aero Modeling (RAM) applied to wind tunnel testing, RAM-T, is an approach to efficiently and automatically obtain aerodynamic models during testing. The approach saves time and resources by responding to the demand for experimental efficiency and model fidelity. Motivation for this demand is more acute when investigating a class of vehicles categorized as Urban Air Mobility (UAM) aircraft where many features from both aircraft and rotorcraft are present. RAM-T provides a feedback loop around the test facility to guide the test toward high-fidelity, statistically rigorous aircraft models. The general RAM approach is applicable to computational or physical experiments. It combines concepts from design of experiment theory and aircraft system identification theory that allow the user the freedom to choose, in advance of the test, a specific level of fidelity in terms of prediction error. RAM only collects data required to meet the user-specified fidelity and fidelity is only limited by the facility and test article capabilities. This paper presents results from tests conducted for development of an automated RAM-T technology. The results highlight some of the unique features of RAM applied to eVTOL configurations.

I. Nomenclature

B_i	=	regression coefficients
C_L, C_D, C_Y	=	lift, drag, and side force coefficients
C_l, C_m, C_n	=	body-axis aerodynamic moment coefficients
e^*	=	normalized residual
e^*_{cv}	=	prediction error metric based on binomial analysis of residuals
F_N, F_A, F_Y	=	body-axis aerodynamic forces, lbf
M_X, M_Y, M_Z	=	body axis aerodynamic moments, ft-lbf
x_i	=	regressors
y	=	response variable in regression equation
α	=	angle-of-attack, deg
β	=	sideslip angle, deg
ε	=	error in regression model

[1] Senior Research Engineer, Dynamic Systems and Control Branch, MS 308, Associate Fellow.
[2] Research Engineer, Flight Dynamics Branch, MS 308, Member.
[3] Research Engineer, Flight Dynamics Branch, MS 308, Member.
[4] Senior Research Engineer, Flight Dynamics Branch, MS 308, Member.

II. Introduction

Aerodynamic modeling for flight dynamics studies plays a key role, particularly for many of the new complex vehicle designs combining features of both conventional aircraft and rotorcraft. Under the Transformational Tools and Technologies Project, NASA is recognizing the need for development of state-of-the-art computational and experimental tools and technologies required for development and prediction of future aircraft performance. Areas developing with increasing interest are in Urban Air Mobility (UAM), distributed electric propulsion, hybrid turboelectric systems, and electric vertical takeoff and landing (eVTOL) configurations. These configurations present more aircraft complexity resulting in substantially more interacting factors and aerodynamic nonlinearities. Traditional experimental methods applied to UAM vehicles can lead to increased costs and missed interactions. Market studies supported by NASA highlight the opportunities and difficulties for these areas both in terms of economics and technology [1-2].

The new design space offers significant opportunities, but it also creates vehicles with substantially more complex and nonlinear aerodynamic responses, as well as increased complex interactions among propulsion and aerodynamic control systems [3]. Resources required for modeling depend on the design stage considered where the levels of model fidelity typically increase as the design progresses. In early design stages for UAM vehicles where lower fidelity may be sufficient, the presence of rotors, propellers, wings, control surfaces, and fuselage result in a greater number of factors to consider, thus, contributing to significant design complexity. This can limit the ease of design changes while advancing through various design stages. Although advances in computer technology have facilitated more effective tools to tackle these issues, obtaining greater model fidelity still requires a significant investment of engineering time and resources both analytically and experimentally. Several research efforts to improve fidelity and efficiency have been made in ground-based testing [4-12], flight testing [13-18], and in computational methods [18-28]. The authors are also supporting current research by NASA in the UAM area [29-35].

In a preliminary study of the RAM concept [34], consideration was given to determine potential metrics, algorithms, and procedures that would allow the RAM process to be implemented in an automated fashion. Experiments were performed on a conventional, off-the-shelf, radio-controlled model aircraft over a large flight envelope. These experiments followed the general RAM process; however, the process was guided manually without any automated decisions. The model, called the “Mini E-1,” is shown in Fig. 1. The experiment successfully evaluated and determined candidate procedures and metrics that support the RAM concept applied in a wind tunnel experiment, or a “RAM-T” application. Results indicated that a sequential automated testing process is possible and can efficiently produce models with statistically rigorous results by limiting the amount of data collected to that needed to achieve user-defined levels of fidelity, specified in terms of prediction errors.

Figure 1. Conventional aircraft (Mini E-1) in the NASA Langley 12-Foot Low Speed Tunnel.

In this paper, a fully automated RAM process is demonstrated by applying the RAM code to measurements from two wind-tunnel tests or “RAM-T” experiments. The first RAM-T demonstration uses a conventional airplane, the Mini E-1, to confirm the hypothesis from the preliminary experiment. The second demonstration uses RAM-T to develop aerodynamic models for an eVTOL tandem tilt-wing design, in a simulated wind-tunnel test. The design proposed by NASA [29] is called the NASA Langley Aerodrome No. 8 (LA-8), as shown in Fig. 2.

In Ref. [32], parts of the RAM process are also applied to LA-8 to investigate candidate model structures and system identification methods for a complex eVTOL configuration. A fully automated RAM-C process is also demonstrated in Ref. [35] using the hybrid rotorcraft-airplane vehicle proposed by NASA [36], called the Lift+Cruise (L+C). The L+C vehicle, shown in Fig. 3, is representative of some of the many complex vehicles being proposed for future UAM missions. Application of RAM-T and RAM-C to various configurations with combined airplane and rotorcraft features is an area of current research.

Figure 2. UAM aircraft configuration (LA-8) in the NASA Langley 12-Foot Low-Speed Tunnel.

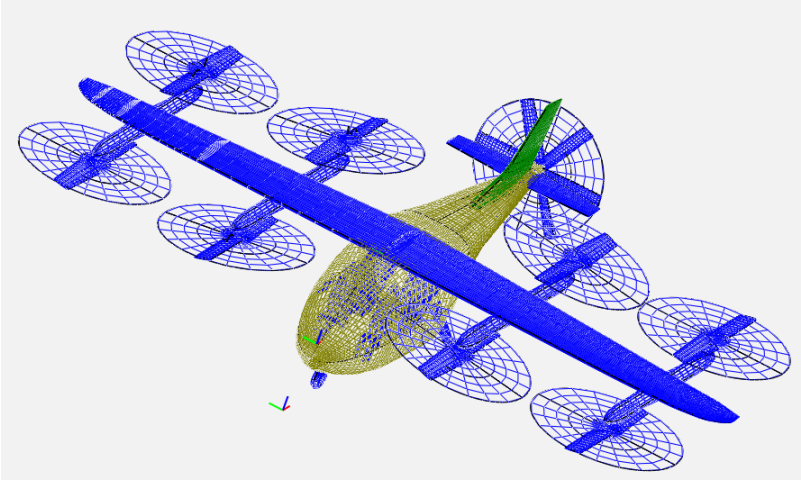

Figure 3. Lift+Cruise, a candidate research design for the UAM airspace.

III. The General RAM Process

One approach to improving the modeling process that reduces the various complexity issues, resource demands, and other adverse impacts described above is through development of a testing process called RAM. Although RAM can effectively be used to develop aerodynamic models of aircraft in general, a primary objective for RAM is to facilitate modeling of complex vehicle configurations intended for UAM applications and that the resulting models are suitable for nonlinear, flight dynamics and controls simulations. RAM capitalizes on fundamentals from design of experiment (DOE), response surface methods (RSM), and aircraft system identification (SID) theory to form a unique automated modeling process. In addition to automating the modeling process while still allowing a subject-matter expert (SME) to retain control, it offers an opportunity for significant savings in time and resources.

An overview of the general RAM concept is presented in Fig. 4 as a simplified flow chart. On the left is the user-desired level of model fidelity and a sequence of pre-designed experiments, in the form of sequential DOE/RSM

blocks of test points, appropriate for the vehicle under test. As the test facility processes each block to produce measurements for model identification, the resulting stepwise regression and Analysis of Variance (ANOVA) tables characterize the relative significance of model terms and other sources of variation. Effectively, the RAM process provides a control loop around the vehicle under test that guides the test through a series of data blocks that are used to estimate models and evaluate their performance. The series of data blocks takes advantage of the sequential nature of designed experiments and only requests more data if it is needed for either estimating a higher-order model or for more detailed investigation in a region where model performance is inadequate. The test is completed when model validation tests are passed, indicating the requested level of fidelity is achieved, or the test may conclude when the limits of the test apparatus measurement capabilities are reached. Replicated test points provide indications of test facility (TF) capabilities in terms of repeatability and precision limitations. Maximum achievable fidelity is limited by the accuracy and measurement capabilities of the test apparatus and physical model under test, or in the case of RAM-C, the CFD methodology and fidelity of the geometry model. The choice of identification methods, prediction error metrics, or how the test regions are split is not restricted by the general RAM process.

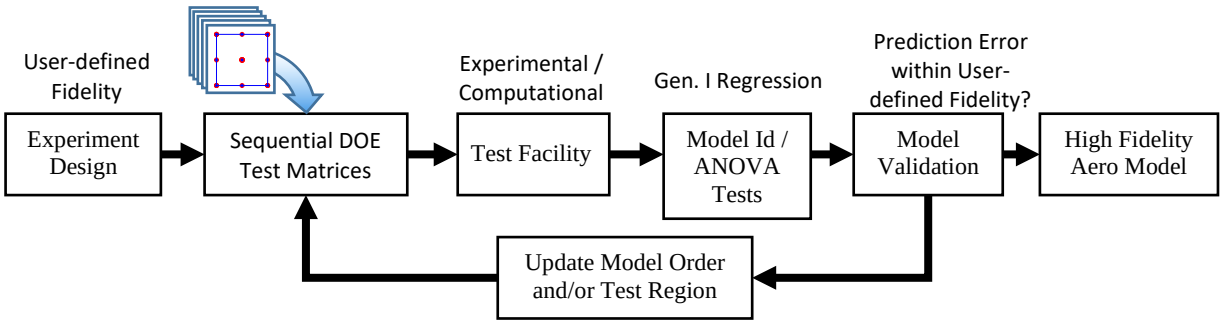

Figure 4. An overview of the RAM process.

Conventional experiments have been designed for use in wind tunnels and flight test for many years. Many of these practices are well established and have been demonstrated and corroborated through cross-comparisons with other tunnels, flight test, and computational methods. This traditional approach typically involves a controlled environment where one-factor-at-a-time (OFAT) methods are used to sweep over one of the one of the states or controls of the vehicle under test while all other factors are held constant. Statisticians will disagree with the OFAT approach due to the possibility of unknown systematic errors being confounded with the data; however, practitioners go to great lengths to ensure that at least known systematic errors are minimized or eliminated. Conventional techniques have traditionally worked well for cases where the number of factors is limited to basic control surfaces and propulsion systems. However, for modern UAM designs, the number of factors can be anywhere from three to five times the number of traditional factors. This quickly degrades a conventional experiment design and limits the test from capturing possibly unexpected factor interactions as well as higher-order nonlinearities in any practical manner or time frame. This is issue is especially acute when time and resources are limited.

In the RAM approach the severity of these issues is reduced, if not eliminated, by taking advantage of well-established theory for model identification and experiment design. DOE/RSM theory is well documented and established in academia, industry, and government for a variety of applications. Credit for initial development of DOE is often given to Fisher [37]. DOE/RSM has since expanded and modernized from Fisher's early agricultural applications to all fields of modern science and engineering.

A. RAM Flow Chart

The general RAM algorithm is presented in Fig. 5 as a flow chart. To avoid confusion between flow-chart blocks and RAM data blocks, the flow chart blocks (FCB) are referred to using notation FCB (#). On the upper left are FCB (1-2) showing the general script for running RAM and a place for user inputs. User inputs define test features such as the factors, factor ranges, and user-desired level of model fidelity. FCB (3) provides a library of unique pre-designed test matrices, in sets of five test-matrix blocks or RAM data blocks, where each set is uniquely defined based on the number of factors involved for the test. These data blocks guide experiments through sequential, optimized test points, where the sequence is designed to accommodate progressively more complicated models and minimize prediction errors. The sequential nature of the RAM process allows data collection to occur only when it is needed for either

estimating a higher-order model or for a more detailed investigation in sub-regions where model performance is inadequate.

RiBjMk is used in the flow chart as an acronym to keep track of the ith-region being modeled, jth-data block under test, and kth aircraft mode currently being evaluated. Aircraft modes are sometimes used to reflect significant configuration or mission changes such as speed regimes for vertical flight versus cruise flight. Details of the data blocks are given in Sec. III.B. In Fig. 5, FCB (4) converts the generic data blocks to reflect the initial factor ranges specified by the user. This block also adjusts factor ranges when the regions under test are required to be split. FCB (5) converts the RAM information into a form appropriate for the test facility (TF). The test facility may be a wind-tunnel (WT), computational fluid dynamics (CFD), or simulated experiment (Sim), as shown in FCB (6). FCB (7) provides the conversion back from TF to RAM. FCB (8) denotes the user selected model identification procedure. For this study, stepwise regression is used and discussed further in Sec. III.C. FCB (8) provides substantial output to the user (FCB (8a), (8b), and (8c)) for monitoring progress of the modeling process. Outputs from the stepwise regression and Analysis of Variance (ANOVA) tables provide key statistics and characterize the relative significance of model terms.

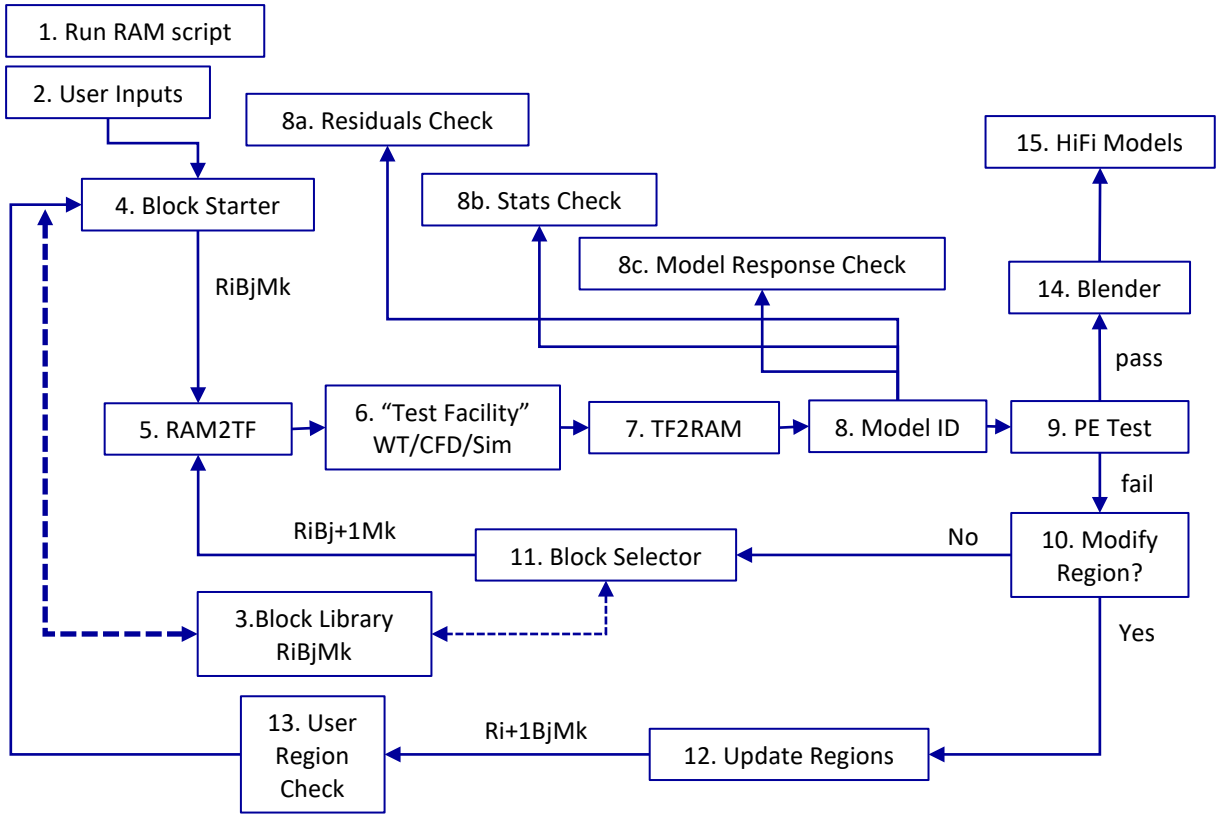

Figure 5. RAM process.

The next step in the RAM process is depicted in FCB (9). This block applies a prediction error (PE) test based on validation data not used for estimation. The PE test determines the progression of the RAM algorithm. If the PE test is passed, meaning the user-defined fidelity has been satisfied, then the final global model is estimated. The final model represents a blending, FCB (14), over all the regions that may have been split during model identification. The results in FCB (15), indicate high fidelity (HiFi) models have been achieved. If the PE test fails, then a decision is made to either use the next RAM data block (test matrix) or split the region under test. The current version of RAM uses five data blocks are used in sequence to reflect a progression from low-order models to high-order models. After each data block, the RAM process uses the PE test to determine if more data is required, reflecting the need to estimate a higher-order model. In this study, polynomial models are limited up to third order. If the test in FCB (10) determines that all DOE blocks have not been used, then RAM proceeds to FCB (11) to obtain the next block. If the test in FCB (10) determines that all data blocks have been used, then RAM proceeds to FCB (12) to split the regions under study. Before proceeding back to FCB (4) to obtain the next test matrices, FCB (13) provides users an opportunity to check

or adjust the RAM progression. The selection of optimal region partitioning is a current area of research [49] that can add value to future RAM versions. The final model represents a blending, FCB (14), over all the regions that may have been split during the RAM process. Individual models covering a subset of the factor space usually do not perfectly intersect with neighboring models at their boundaries, which creates a discontinuity between modeling regions. In order to blend neighboring models, the RAM software utilizes data from regions on both sides of the model intersection to create additional models spanning over the local intersections. The regions of overlap between local models are then smoothly combined using a polynomial weighting function.

B. Experiment Design

In advance of performing an experiment, application of the well-developed DOE/RSM concepts provide guidance on setting up an efficient and statistically rigorous test plan as well as providing a much higher probability of obtaining an adequate model. For a RAM-based study, DOE/RSM theory is used to develop a specialized series of test matrices or data blocks that are applied in sequence. These data blocks are stored in the RAM Block Library and are constructed in coded space to improve numerical calculations and to allow more general application as factor ranges vary for each region tested. Ref. [32] expands on other considerations when using this approach. Coded form scales all the factors to lie in the range [-1, +1], as shown in Eq. (1).

$$\tilde{x} = \frac{x - (x_{\min} + x_{\max})/2}{(x_{\max} - x_{\min})/2} \tag{1}$$

For the current studies, RAM aerodynamic models use a polynomial model structure, although other model structures could be applied as well. In general, experiment design based on DOE is well documented in Ref. [39]. Five key principles of DOE support RAM and the sequential process to testing and modeling. The principles commonly used in DOE design are:

1. Orthogonal regressors – uncorrelated regressors to improve estimation calculations.
2. Replication – independent and repeated measurements to assess system noise and uncertainty.
3. Randomization – randomized input matrix to average out extraneous factors and unknown systematic errors.
4. Blocking – technique to improve precision and reduce variability due to known nuisance factors.
5. Sequential testing – a knowledge building process that allows each step to benefit from the previous one.

These principles provide important benefits to any designed experiment. In RAM experiments blocking and sequential testing serve additional purposes beyond basic DOE designs. For DOE tests in general, the concept of blocking serves to reduce miscellaneous nuisance bias errors, such as from different tunnel operators or different days of operations. Spreading out runs over additional blocks has also been useful in avoiding tunnel overheating where particularly large blocks require very long runs. However, an additional and primary purpose for the RAM sequential blocks of data is to perform sequential model identification that progresses from low-order models to higher-order models. Model identification allows only up to third-order polynomials and three-factor interactions. These higher-order terms typically appear in very limited numbers and, given the amount of data collected in a RAM process, the number of degrees of freedom for estimation is very high. As in any modeling process, final review of model terms is always required by SMEs to ensure the estimated coefficients make sense for the application. Ref. [35] describes specialization of RAM block designs for experiments using computational or analytical methods as the test facility.

One classical DOE design is the factorial experiment [37]. A factorial design is one which varies all factors at the high and low level for all possible combinations. Using two levels for each factor represents a run-efficient method for developing a model that includes first order and 2-factor interaction terms. A full-factorial design in two-factor space is shown below in Fig. 6 with the addition of a center point.

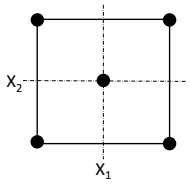

Figure 6. A full-factorial design in two-factor space.

Replicated centers allow testing for curvature that may suggest further augmentation is required to support quadratic model terms. This type of information allows the investigator to sequentially build models and only incorporate increasing amounts of data as required. The supported regression model is shown in Eq. (2) with up to two-factor interactions (2FI) as

$$y = B_0 + \sum_i B_i x_i + \sum \sum_{i \neq j} B_{ij} x_i x_j + ... + \varepsilon \qquad i = 1, 2, ..., k \tag{2}$$

The B_i, B_{ij}, are the fitted regression coefficients and the x_i are the factors (independent variables or regressors). A refinement (augmentation) to the factorial design is the central composite design (CCD) [40] which adds design points along the axes through the origin of the design space as shown by the square symbols of Fig. 7. The location of the axial points defines this CCD as a face-centered design (FCD).

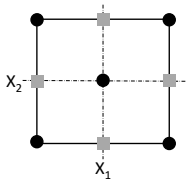

Figure 7. A face-centered central composite design in two-factor space.

This approach supports a full second order model given in Eq. (3).

$$y = B_0 + \sum_i B_i x_i + \sum_i B_{ii} x_i^2 + \sum \sum_{i \neq j} B_{ij} x_i x_j + \varepsilon \qquad i = 1, 2, ..., k \tag{3}$$

The nested face-centered design in two-factor space, shown in Fig. 8, allows the nesting of two FCD designs to support the addition of pure cubic terms to the empirical model. The two FCD's may be tuned by fractionating the factorial designs as presented by Landman et al. in Ref. [7]. The nested FCD is particularly useful in aerospace applications where nonlinear responses due to control surface deflections can occur. The design ensures the full range of each surface is covered and provides a minimum of five test points for each factor. The supported model is given by Eq. (4).

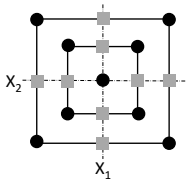

Figure 8. A nested face-centered design in two-factor space.

$$y = B_0 + \sum_i B_i x_i + \sum_i B_{ii} x_i^2 + \sum \sum_{i \neq j} B_{ij} x_i x_j + \sum_i B_{iii} x_i^3 + \varepsilon \qquad i = 1, 2, ..., k \tag{4}$$

RAM data blocks are developed as sequences of five blocks: (1) FCD, (2) nested FCD, (3) an I-optimal designs that minimize prediction error for quadratic models, (4) I-optimal designs that minimize prediction error for up to cubic models, and (5) a final block to obtain validation data. The validation block can be applied separately at any point during the test but generally is taken at the start to allow validation tests throughout the experiment. After the nested FCD, the series of I-optimal blocks vary in size depending on the number of factors involved. The design choice of using five blocks is not a requirement but the authors have found it to be a reasonable choice for many cases. The series of blocks represent a progression of data collection required to allow models from linear+2FI polynomials up to and including cubic+3FI. For cases with large numbers of factors, optimization to minimize prediction error can require machines with parallel processing capabilities. In cases where computational power is limited, the user may select a reduced-cubic model where an SME may assist in selecting key cubic or 3FI terms as appropriate.

Using polynomial model structures, limited to a maximum of cubic+3FI terms, quickly leads to a requirement for dividing the global-model range into smaller regions. Polynomial models with higher-order terms than cubic can lead to parameter estimation problems and undesirable response and slope changes near the region end points. Fortunately, higher-order polynomials are unnecessary using the RAM splitting process. Splitting regions is performed on dominant factors with strong aerodynamic nonlinearities such as angle of attack for conventional aircraft and velocity for rotorcraft. The split regions are blended in the final steps of RAM to provide continuous and smooth connections between split regions. The blending process uses data from both sides of the split to create an additional model spanning the local region intersection. The local models are smoothly combined using a quintic transition polynomial weighting function, following the similar procedures to those described in Ref. [33].

C. Model Identification

The general process of guiding model identification in RAM was outlined in Sec. III.A and it is applicable to both computational and physical test environments. A commonly used process for aircraft model identification was described briefly in the previous RAM study [34] and more generally in Ref. [38], where the model identification methods used in RAM were adapted from the accompanying System IDentification Programs for AirCraft (SIDPAC) software toolbox. For models developed in this study, model identification (specifically model structure determination and parameter estimation) is accomplished using stepwise regression. This is a well-known method and broadly used in many science and engineering applications. However, the RAM process does not restrict the user to a single method of model structure determination and parameter estimation. The process is improved for eVTOL configurations using models where the aerodynamic responses are defined in dimensional form and ranges for freestream velocity are defined in terms of body-axis velocities [32]. This approach allows more straightforward modeling of flight conditions representing slow transition, vertical, and hover flight, where freestream velocity can be zero or very small. However, for conventional airplane configurations nondimensional aerodynamic coefficients are preferred.

D. Validation

Three key objectives in the RAM modeling process are: (1) minimize standard error to get an adequate model fit, (2) minimize prediction error to get a useful model, and (3) only collect enough data to meet the precision, prediction, and validation requirements. These objectives reflect a balance among the precision demanded by the experimentalist, the capabilities or precision levels possible by the test apparatus, and the time and cost required to meet those demands. The basic goal is to expand data collection only enough to meet the model complexity requirements. The validation step supports these objectives.

Validation is a key step (FCB 9) in the RAM process used to test model performance. This step determines whether the estimated model is a good predictor of the system responses within user-defined bounds. A practical method for assessing validation is to observe the residuals between measured and predicted responses on data not used for estimation. For well-designed experiments that result in adequate models, the residuals appear as white noise with magnitudes generally within the specified acceptable levels. Not every residual test point will meet the acceptable error boundary limit, however. As described in Ref. [41], success or failure of a given validation test-point residual to meet the requirement can be judged as a binomial (pass-fail) experiment. For complex vehicle tests where large numbers of data points are required, the RAM process typically utilizes 75 test points for validation. In that case, the critical binomial number is 66, based on models estimated at a 95% confidence level, and allowing only 1% inference error in the binomial test. This implies that the worst nine validation residuals define the level for an adequate model. The PE test metric and the general simulated test case are discussed for RAM-C in Ref. [35].

For physical experiments, the PE test metric is formed by using normalized residual errors from validation data and satisfying the binomial test. The normalized residual error is defined as the difference between the response variable and the model predicted value, normalized by the maximum absolute value of the response variable, as shown in Eq. (5). An alternative is to normalize by the full range of response, demonstrated in [32].

$$e^* = \frac{z - \hat{y}}{\max(|z|)} \tag{5}$$

The normalized residual provides a metric conveniently describing the relative success of the modeling process. The PE test metric is then based on the normalized residual errors (in ranked order) that satisfy the binomial test. Eq. (6), indicates a level determined by the critical binomial number, *B*.

$$e^*_{cv} = e^*(B) \tag{6}$$

IV. RAM Modeling Experiments

Two modeling experiments are provided in this study. These tests were designed to the demonstrate accuracy and efficiency of the automated RAM-T process and confirm the modeling results produced in the preliminary study [31]. The two aircraft configurations tested are the Mini E-1, representing a conventional fixed-wing aircraft configuration, and the LA-8, representing a complex UAM configuration. Results for the Mini E-1 demonstration are obtained using data directly from testing in the NASA Langley 12-Foot Low-Speed Tunnel (12-ft LST). The preliminary Mini E-1 experiment [34] was not performed in an automated fashion however the testing process followed the RAM-T process exactly and produced data that can be used in this study to demonstrate an automated RAM-T process based on experimental data. Results for the LA-8 demonstration are produced through simulated wind-tunnel experiments. The simulation model in this case utilizes strip theory-based tilt-wing aerodynamic calculations [50] combined with high-fidelity LA-8 propeller models identified from isolated propeller wind tunnel testing [33]. The full simulation model gives predictions representative of an aircraft conceptual design tool and includes predictions for complex high-incidence angle propeller aerodynamics and wing-propeller interactions pertinent to modeling tilt-wing vehicles. The simulation output includes noise levels for each response variable representative of that found in a wind tunnel environment.

A. Test Facility

The Langley 12-Foot Low-Speed Tunnel (12-ft LST) facilitated preliminary development of the RAM testing method. The 12-ft LST* is an atmospheric pressure, open circuit tunnel enclosed in a 60-foot diameter sphere. The test section is octagonal with a width and height of 12 feet and a length of 15 feet with each octagonal side measuring 5 feet. The maximum operating pressure is Q = 7 psf (V = 77 ft/sec at standard sea level conditions), which corresponds to a Reynolds number of approximately 492,000 per foot. The longitudinal center-line-flow in the test section has a turbulence level of about 0.6 percent. Test section airflow is produced by a 15.8-ft. diameter, 6-blade drive fan powered by a 280 HP, 600 volts, 600 RPM DC motor. The 12-ft LST is operated from its control room positioned behind the test section and the drive fan. The model can be observed through the large viewing windows or the multiple controllable video cameras.

Models are mounted on a 6-component balance and connected to the tunnel's C strut via a belly-mounted sting. The C Strut allows the attitude of the model to be controlled by the data acquisition system. For the Mini E-1 test, this system was connected to an Arduino mega via a User Datagram Protocol (UDP) internet connection. The Arduino was mounted in the model and commanded one servo on each of the 7 control surfaces. The Arduino sent a pulse width modulation (PWM) command to each servo. It also recorded the actual angular position of the surfaces via 7 encoders, which was then reported back to the data acquisition system. This system removed the need to manually change the position of a control surface between runs. The commanded PWM signals for each servo and encoder output were calibrated from measurements taken at a minimum of 5 different deflection angles. With this system, a run file of the desired model attitude and surface deflection at each data point was able to be loaded into the data acquisition system. The data acquisition system would then command all the needed changes during the run and capture all of the data recorded for the run and report it in a single file. The types of data recorded include, the 6 force and moment components exerted on the model, the commanded and actual positions of the surfaces, the angle of attack and sideslip of the model, and the flow conditions of the tunnel.

B. RAM-T Applied to Mini E-1

Application of a fully automated RAM modeling process to a conventional aircraft, Mini E-1, is presented by utilizing measurements from the preliminary experiment [34]. The preliminary experiment followed the RAM process

* https://researchdirectorate.larc.nasa.gov/12-foot-low-speed-tunnel-12-ft-lst/

and obtained measurements defined by the RAM data blocks. With the data blocks incorporated into the Block Library, an automated RAM experiment is demonstrated, and models are identified using measurements obtained during the experiment. For the current Mini E-1 study, 5 RAM data blocks were acquired from the 9-factor designs in the RAM block library. Results for this study are in the form of a PE test metric and final aerodynamic polynomial models, shown as three-dimensional surfaces.

For conventional wing-tail aircraft configurations, modeling investigations typically define response variables as the aerodynamic model coefficients expressed in nondimensional form and define the explanatory variables in terms of aircraft states and controls. Wind angles are represented by angle of attack and sideslip. For the Mini E-1, the manual RAM-T test was performed in the 12-ft LST at a dynamic pressure of 2 psf while varying angle of attack, angle of sideslip, and control surface deflections. The factors are summarized in Table 1.

Table 1. Factor ranges for Mini E-1 test.

No.	Label	Description	Low	High	Units
			Range	Range	
1	α	Angle of attack	-5	35	deg
2	β	Sideslip	-5	5	deg
3	LA	Left aileron	-30	30	deg
4	LF	Left flap	-30	30	deg
5	RF	Right flap	-30	30	deg
6	RA	Right aileron	-30	30	deg
7	LE	Left elevator	-30	30	deg
8	RE	Right elevator	-30	30	deg
9	RUD	Rudder	-30	30	deg

Table 2. Maximum (worst case) values of design metrics (9 Factors) for Mini E-1.

Block Type	Blocks	Pts.	Design Terms	VIF	FDS	% Power
	(inclusive)					2σ, s/n=2
Minimum Resolution V FCD	1	70	Quadratic	6.72	0.81	80.0
Nested FCD	1, 2	140	Quadratic	10.60	0.95	86.3
I-optimal	1, 2, 3	362	Quadratic	1.53	1.0	99.9
*Mixed (I-opt)	1, …, 4	437	Quadratic	1.46	1.0	99.9
*Mixed (I-opt)	1, …, 4	437	Cubic	25.19	1.0	85.4
Validation (I-opt)	1, …, 5	512	Cubic	24.85	1.0	91.7

*Block 4 can be used for validation or, if needed, provide data for more complex models.

Table 2 shows three example design metrics used for each block. Additional details of the design process are discussed in [34]. Three design metrics, Variance Inflation Factor (VIF), Fraction of Design Space (FDS), and experimental power, demonstrate the progressive nature of the RAM data blocks. VIF reflects the degree of orthogonality for the regressors with values of 1 indicating perfect orthogonality and values over 10 reflecting some degradation in certain regressors that may require further design evaluations. FDS is a graphic tool for evaluating the standard error profile over the design space. The number reflects the fraction of the design space within the expected variance parameters. For the design process, an assumption is made that standard deviation is 1 to allow relative predictive error to be computed. The RAM designs use a very conservative assumption that the signal-to-noise ratio is only 2. The last metric, experimental power, used to avoid type 2 errors, is acceptable for values over 80%. Maximum values of the design metrics were selected from a survey of all model terms to show how each block design was progressing and improving the overall design as blocks of additional design points were added.

The first three of five blocks present a sequence of designs: FCD, nested FCD, and I-optimal that highlight the benefit of an I-optimal design. I-optimal designs are based on minimizing the integrated prediction variance over the design space. Each block was designed assuming a full quadratic model and each step provided more degrees of freedom for a more complex model, if needed. The VIF values in data block 2 show the cost of adding a nested FCD in order to capture potential nonlinearities as expressed in Eq. (3). The third block is an I-optimal design that minimizes prediction error. This block strategically added 222 test points and improved the statistical design metrics. The first three blocks are expected to allow adequate modeling of the aerodynamic coefficients, especially in the lower angle-

of-attack region below stall, where models were expected to be almost linear or mildly quadratic. Block 4 provides additional I-optimal modeling data, if needed, to satisfy greater model complexity demands. Block 5 is also an optimal design but only used for validation tests. The optimal blocks are useful for validation data since the optimizer avoids using existing design points. In Table 2, block 4 is also shown applied to both quadratic models and cubic models. The degradation to the experiment design of adding block 4 to the cubic case is relatively small since the FDS metric, the preferred metric for response surface modeling, is still satisfactory.

Figure 9 presents the nine-factor, full angle-of-attack range, RAM block designs for Mini E-1, viewed as a function of angle of attack and sideslip. The graphic on the left shows only the first two blocks: the basic FCD (red squares) and the nested FCD (green squares). The graphic on the right shows all five blocks together. The last three block (blue, gray, purple, respectively) are the I-optimal points. Similar plots of design points are obtained by plotting any two of the nine factors. The I-optimal blocks increase the data density and allow increased model complexity as needed. Since the I-optimal points are optimized to reduce prediction error there is a strong preference toward the boundaries of the region tested. This is expected since model errors are typically best in the factor mid-ranges and progressively degraded toward the edges of the tested regions.

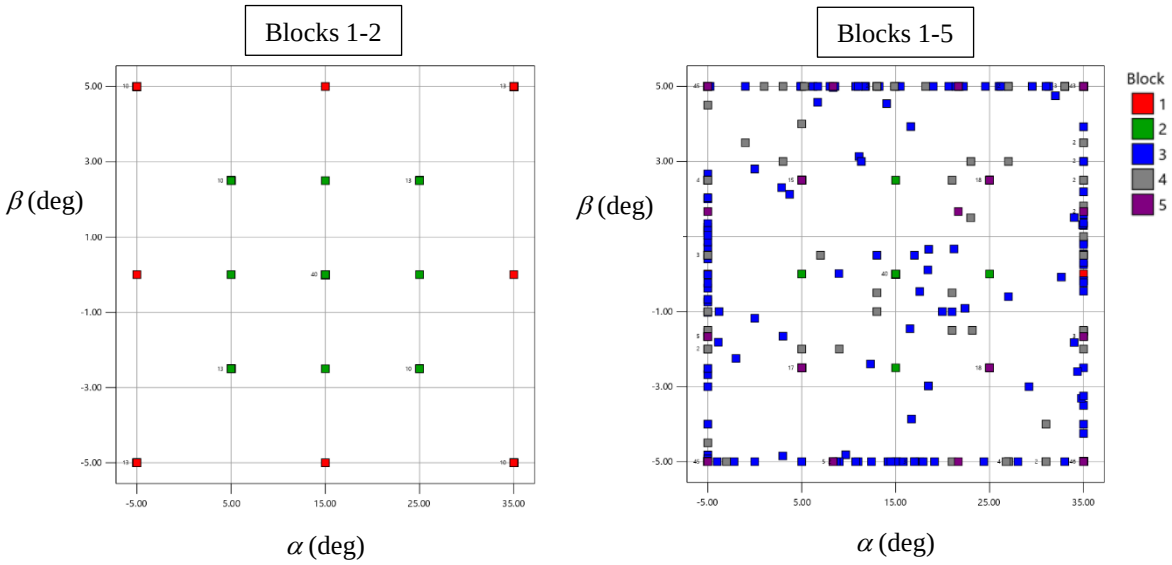

Figure 9. DOE block designs for RAM.

In the experiment design phase, the investigator must define the confidence level required, signal/noise ratio for the test apparatus, and the minimum level of response detection required. However, for the execution phase, the investigator must also pre-define a level of acceptable prediction error for validation tests to confirm an adequate model and prevent over-collecting data.

At the start of the test, the ranges set for each factor define the first region, R1. During the test, if progression through all 5 blocks of data is still insufficient to meet the pre-defined fidelity levels, then the test ranges can be adjusted to smaller regions. The choice for this study was to simply split the regions in terms of angle of attack until a satisfactory prediction error was obtained. The choice of angle of attack to determine regions reflects the dominant role it plays in aerodynamic response.

Figure 10 shows the splitting sequence used in this study of the Mini E-1. The widest region with the largest factor ranges is R1. The split of R1 on level 1 (L1) results in two new regions R2 and R3 on level 2 (L2), and so on. To assist the investigators using RAM, statistical information is continuously provided for each sub-region and when a split is required the user is given additional global model statistics to evaluate before proceeding. The RAM process continues until the PE metrics for each coefficient are satisfied or the user decides the models are adequate. Additional testing efficiencies can occur in an automated RAM process by virtue of the splitting process. Once data are collected for a region to be split, the sub-regions already have a substantial amount of data required for that new region. In future versions of RAM, the data already collected in a sub-region need not be repeated.

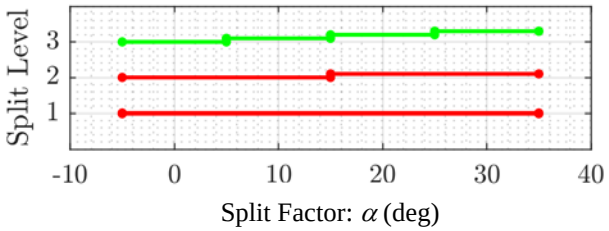

Figure 10. RAM test-region splits for Mini E-1.

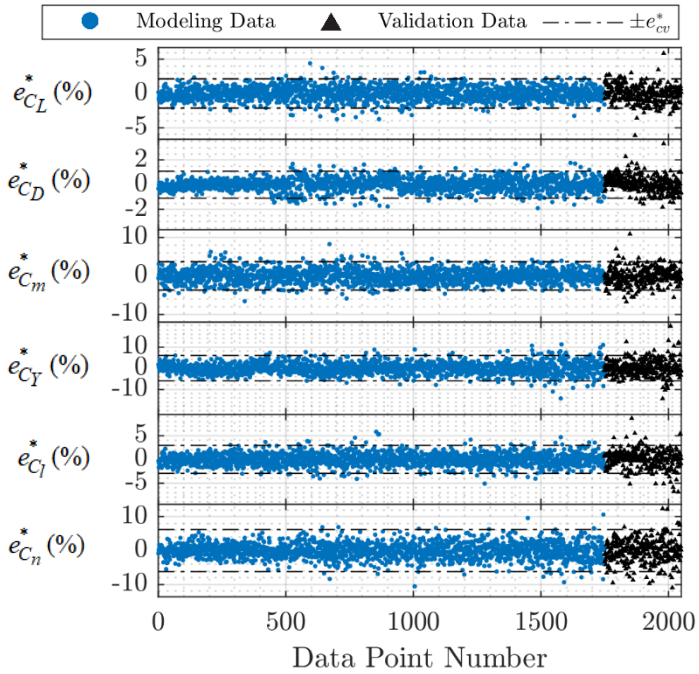

Figure 11. Normalized residuals at completion of RAM test for Mini E-1.

Figure 11 shows the final normalized residuals (defined in Sec. III.D) for each aerodynamic coefficient after the experiment is completed over three split levels and data taken at seven separate regions. Residuals in Fig. 11 confirm the quality of the models by presenting a zero mean, constant variance process. Figure 12 presents the PE metric (expressed as a percentage) obtained at each split level for each coefficient. The PE metric values indicate with model identification at Level 3, the prediction errors are less than 5% for each coefficient except for C_Y and C_n, which are approximately at 6%. At this point the models were deemed adequate, however if greater performance were required then the RAM-T process could be continued. Further splitting reduces the range that polynomial models must cover and increases the data density within the new regions.

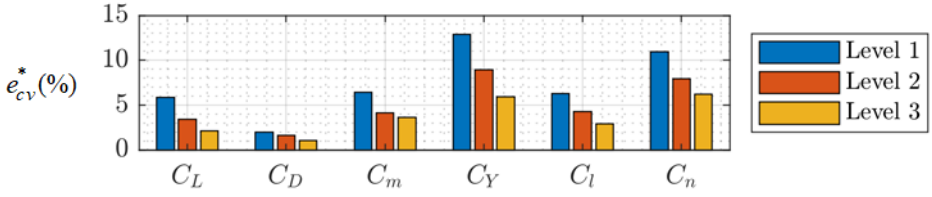

Figure 12. PE metric for each split level.

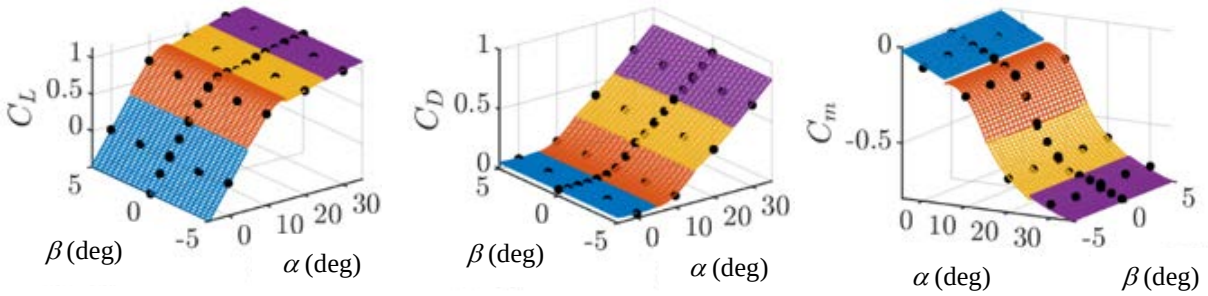

Figure 13. Split sub-region longitudinal models for Mini E-1.

As representative model examples, the longitudinal coefficients are presented in Fig. 13. The figure shows four sub-regions modeled at split level 3 (L3). The black dots show measured data for comparison with the model surfaces. To make the plots more tractable, measured data points are selected for the plot only at the mid-range values of each factor. Since it is difficult to obtain a smooth transition between regions due to the nature of polynomial fits estimated for each region separately, the model blending approach described in Sec. III.A is used to create a globally smooth and continuous response surface. The polynomial fits used to blend the models covering each region are shown in Fig. 14. Figure 15 presents the final global models for the entire range of factors investigated.

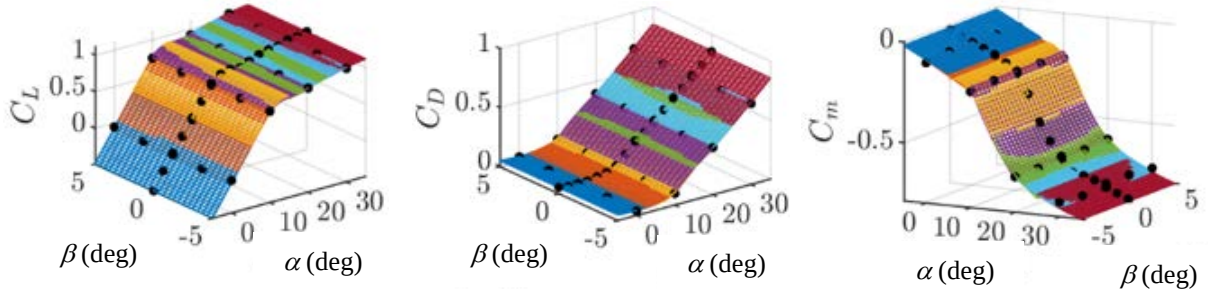

Figure 14. Blended sub-region longitudinal models for Mini E-1.

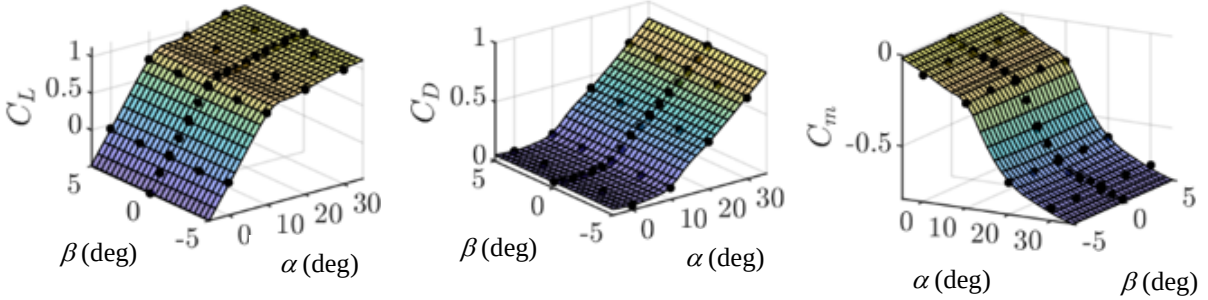

Figure 15. Longitudinal global models for Mini E-1.

C. RAM-T Applied to LA-8

Results of an automated RAM modeling process applied to a complex configuration, LA-8, are provided in this section. Results highlight experiment design, prediction error metrics obtained during the experiment, and the final aerodynamic polynomial models, shown as three-dimensional surfaces. The demonstration is produced through simulated experiments where the modeled LA-8 components included the fuselage, two rotating wings, v-tail, four elevons, four flaps, two ruddervators, and eight wing-mounted propellers with geometry and placement modeled after a 62 lb. wind tunnel and flight test vehicle [14]. Other smaller components, such as winglets and propeller support struts, are not included in the model. The semi-empirical simulation model utilizes strip theory-based tilt-wing aerodynamic calculations [50] combined with high-fidelity LA-8 propeller models identified from isolated propeller

wind tunnel testing [33]. The simulation output includes noise levels for each response variable representative of that found in a wind tunnel environment.

The following are the simulated LA-8 wind tunnel test assumptions regarding the measured quantities. Values are chosen to be representative of the wind tunnel test environment.

- Standard day atmospheric conditions.
- Force and moment measurements are corrupted by zero-mean, Gaussian, white noise and have no drift. The measurement noise standard deviations are 0.15 lbf for F_A, 0.15 lbf for F_Y, 0.50 lbf for F_N, 0.30 ft-lbf for M_x, 0.75 ft-lbf for M_y, and 0.15 ft-lbf for M_z. These numbers reflect the measurement variance observed in previous LA-8 wind tunnel entries [30].

Table 3. Factor ranges for the LA-8 test at Q=3.5 psf.

No.	Factor	Units	Low	High
1	α	deg	-5	10
2	β	deg	-5	5
3	δw (W_1, W_2 ganged)	deg	0	40
4-7	F_1-F_4	deg	0	40
8-11	E_1-E_4	deg	-25	25
12-13	R_1-R_2	deg	-30	30
14-21	N_1-N_8	rpm	3700	6000

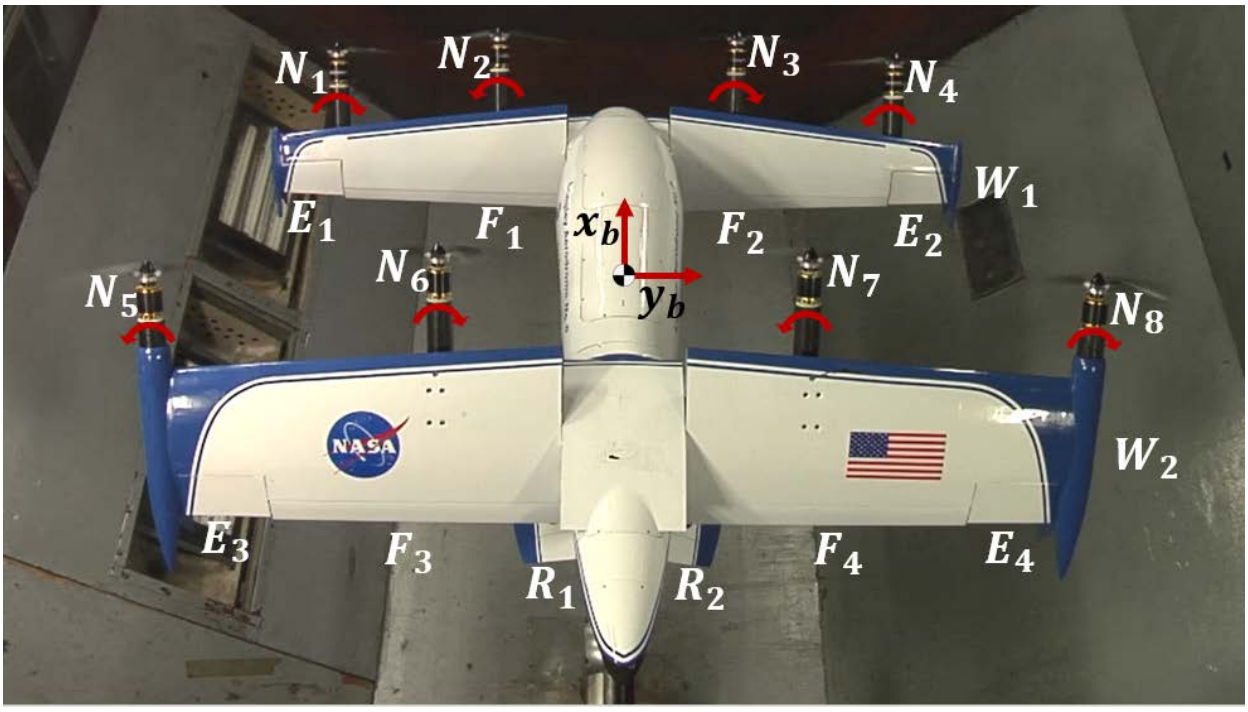

Figure 16. LA-8 propulsion and control surfaces.

Supporting the current study, a manual RAM-T test was performed in the 12-ft LST after a conventional set of exploratory tests [30, 31]. Based on the exploratory experiments [30] it was possible to define more accurately the factor ranges in a transition flight regime and provide more data density in a RAM-based experiment. For the simulated example in this study, to demonstrate the RAM process, a mid-range Q was selected as representative of the complex transition region between vertical and horizontal flight. The test space for LA-8, operating at Q = 3.5 psf, is summarized in Table 3. In this case 21 factors can vary during the RAM-T experiment. The aerodynamic orientation

of the vehicle is defined by angle of attack (α) and sideslip (β). The remaining 19 propulsion and controls are shown in Fig. 16. In Table 3, the two independent wing tilt angles are labeled W_1 and W_2. For this study they are ganged together and operate on one commanded position. Flaps are labeled as F_1 to F_4. Elevons are labeled as E_1 to E_4. The eight rotors are labeled as N_1 to N_8. Ruddervators, R_1 and R_2, are only slightly visible in Fig. 16, located at the bottom of the figure under the fuselage.

Design metrics for this experiment are shown in Table 4. In the same fashion as developed for the Mini E-1, the worst-case metrics were selected from a survey of all model terms to show how each block design was progressing and improving the overall experiment design as blocks of additional design points were added. The design blocks represent a sequence of optimized test points facilitating an efficient and statistically rigorous modeling process that seeks to improve experiment design statistics and minimize model prediction error. Although each additional block provides more data and allows a more complex model to be identified, in this case the design objectives were limited to quadratic plus 2-factor interaction terms. This limitation occurs for combinations of very large numbers of factors and higher-order polynomials. In this case, 21 factors in combination with cubic-order plus 3-factor interactions, produces a very large number of terms that are required to be optimized in the design process. The required computational power and parallel processing was not used at the time of this study, so polynomial order was limited to quadratic plus 2-factor interactions for these designs. Data block designs limited to quadratic plus two-factor interactions are not a roadblock to the RAM modeling process. However, using lower-order polynomials in the data block designs can lead to a greater amount of region splitting.

The five blocks present a sequence of designs: FCD, nested FCD, and three I-optimal blocks that define the test sequence for a given region. I-optimal designs minimize the integrated prediction variance over the design space. Each block was designed assuming a full quadratic model and each step provided more degrees of freedom for a more complex model, if needed. The VIF values in block 2 show the cost of adding a nested FCD in order to capture potential nonlinearities as expressed in Eq. (3). The nested FCD ensures the full range of each surface is covered and provides a minimum of five test points for each factor. The third block is an I-optimal design that minimizes prediction error. This block strategically added 120 test points to substantially improve the design metrics. Block 4, in this case, provided additional I-optimal modeling data but only slightly improved the VIF design metric. Block 5 provides an optimal design used for validation tests.

Table 4. Maximum (worst case) values of design metrics (21 Factors) for LA-8.

Block Type	Blocks	Pts.	Design Terms	VIF	FDS	% Power
	(inclusive)					2σ, s/n=2
Minimum Resolution V FCD	1	304	Quadratic	19.29	0.09	79.8
Nested FCD	1, 2	608	Quadratic	46.53	0.21	84.5
I-optimal	1, 2, 3	728	Quadratic	6.37	1.0	99.9
*Mixed (I-opt)	1, …, 4	848	Quadratic	3.96	1.0	99.9
Validation (I-opt)	1, …, 5	923	Quadratic	3.29	1.0	99.9

*Block 4 can be used for validation or, if needed, provide data for more complex models.

Figure 17 presents the 21-factor 5-block design for LA-8. The graphic is presented as a 2-dimensional slice into a 21-factor space and shows the design points as a function of angle of attack and sideslip. The graphic on the left shows only blocks 1-2 to highlight the differences in the lower blocks. The blocks on the right shows all five blocks together. Although some points appear on top of others, the points are different and represent test points varying with other factors not shown. Similar plots of design points are obtained by plotting any two of the 21 factors. As seen in the designs for Mini E-1, Fig. 9, the I-optimal designs are optimized to reduce prediction error, consequently there is a strong preference toward placing points near the boundaries of the region tested where model prediction errors are typically degraded.

RAM users will start the modeling process by defining the first region (R1) to be addressed which is done by defining the full factor ranges for level 1 (L1). This step may require some exploratory experiments in advance to refine the experiment design and maximize efficiency of testing. As noted previously, if all 5 blocks of data are insufficient to meet prediction error requirements, then the test ranges are adjusted by splitting to smaller regions. For the LA-8 study, this is shown in Fig. 18. In this case, only one split was required to satisfy modeling requirements.

Figure 19 shows the final normalized residuals for the longitudinal aerodynamic forces and moments after the experiment is completed with only two levels and three test regions. As in Fig. 11, the blue circles correspond to data used for estimation and black triangles represent validation data. The normalized residual error, Eq. (5), presents a

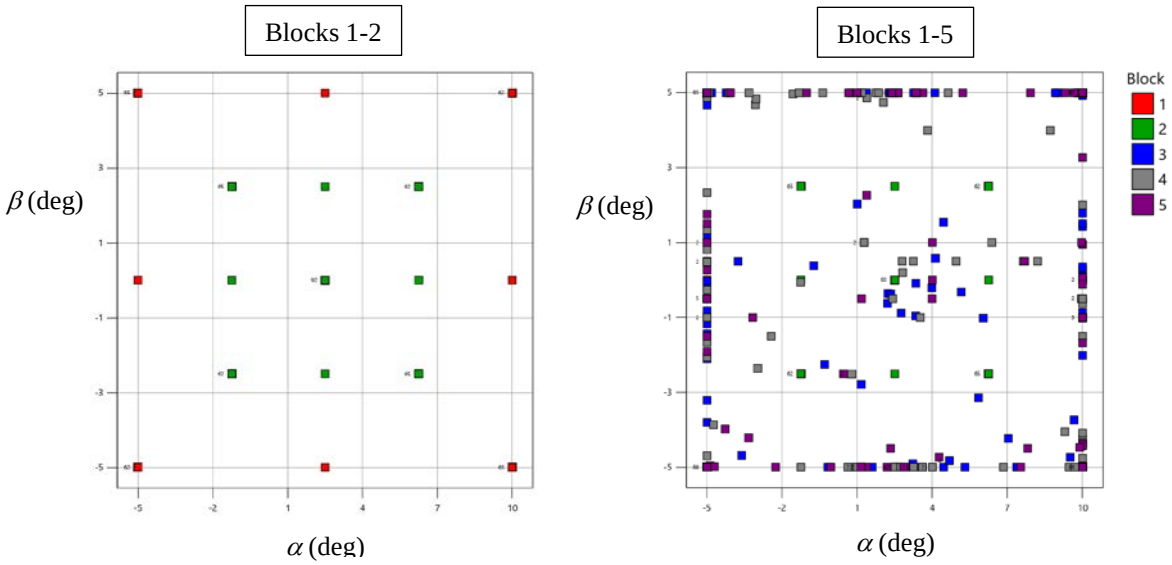

Figure 17. RAM block designs for LA-8 study.

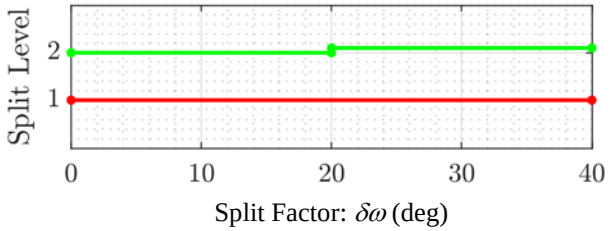

Figure 18. RAM region splits for LA-8 study.

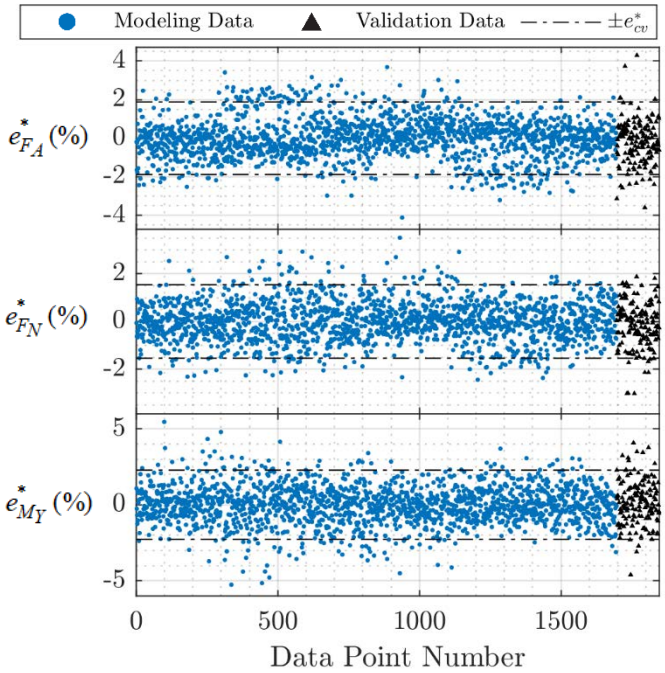

Figure 19. Normalized residuals at completion of RAM test for LA-8.

satisfactory random scatter supporting the quality of the models. The dashed lines show the prediction-error benchmark and indicate that these coefficients have met prediction-error levels well under 3% error.

Figure 20 presents the PE metric (expressed as a percentage) obtained at each split level for each of the six aerodynamic responses. This graphic shows that for the lateral axis, the PE metric for F_Y, M_X, and M_z are approximately 6.8%, 3.4%, and 3.6%, respectively. These results suggest adequate models, especially after only 1 split but engineering judgement would determine if further refinement of the models is necessary. The slightly higher PE for lateral-directional results may reflect limited directional control power in this design [30].

Figure 21 presents the two sub-regions modeled at split level 2 (L2) for the longitudinal coefficients with black dots indicated measured data along mid-range factor values. The model coefficients are plotted against angle of attack and combined wing-tilt angle (δw) as example response surfaces. Blending between regions is used to ensure continuous and smooth transitions between regions. The response surfaces are used for model blending are shown in Fig. 22. Figure 23 shows the final smooth global model response surfaces for the entire range of factors investigated.

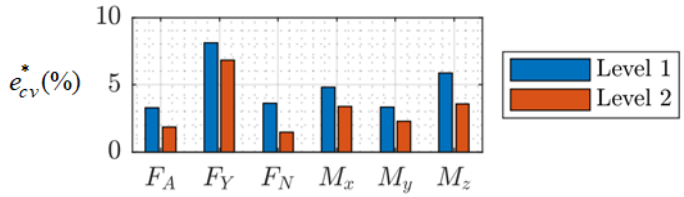

Figure 20. PE metric at each split level for LA-8.

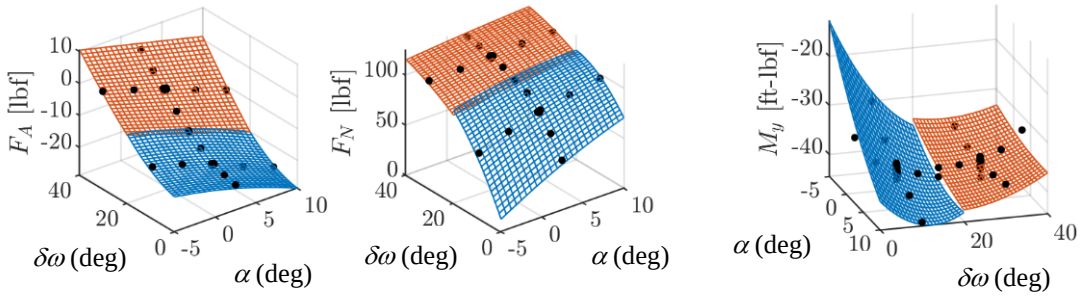

Figure 21. Split sub-region models with center data points for LA-8.

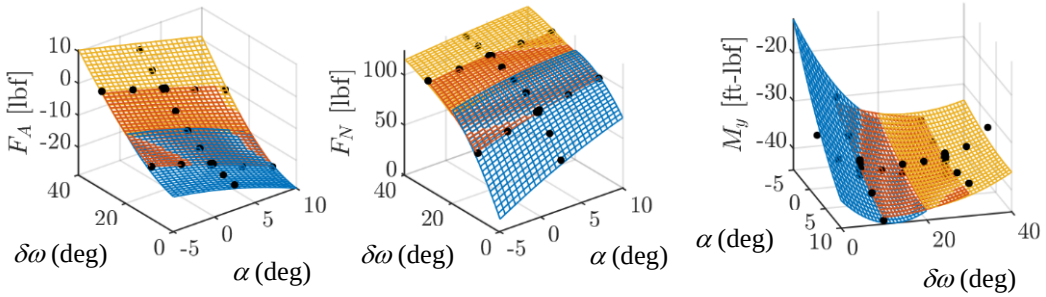

Figure 22. Blended sub-region models with center data points for LA-8.

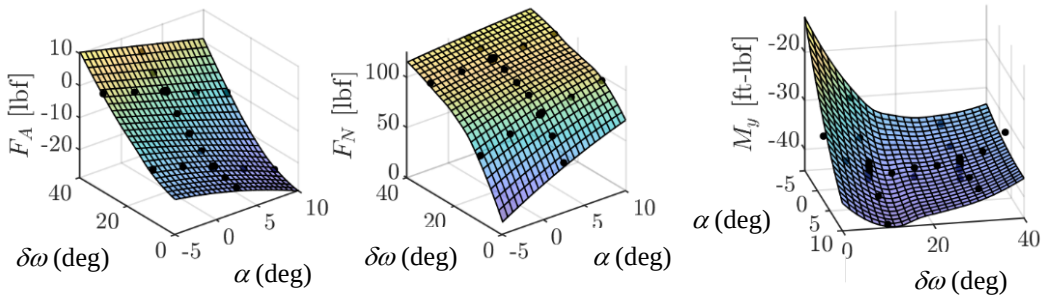

Figure 23. Final global models with center data points for LA-8.

V. Concluding Remarks

Aircraft complexity both in numbers of factors and aerodynamic interactions, for hybrid aircraft-rotorcraft configurations, such as eVTOL, have motivated studies to develop an approach to testing and modeling that can guide the process in a more automated, efficient, and statistically rigorous fashion. The RAM process is an approach that supports that goal and was demonstrated with results from modeling two different aircraft: a conventional aircraft configuration and a complex eVTOL configuration. Designed experiments based on DOE/RSM and system identification theory, in an automated RAM process, can provide statistical information before, during, and after the experiment is completed. The RAM process is particularly helpful to investigators working to obtain a specific desired level of model fidelity. The sequential nature of the RAM approach also inherently limits data collection to that required to match model complexity and fidelity requirements. In addition, for typical eVTOL vehicles where the number of factors may be 3-5 times that of a conventional aircraft, an automated RAM approach provides guidance starting with experiment design, through test execution, and in final model analysis. Examples of RAM-T have demonstrated an automated modeling process for static aerodynamic testing in a wind-tunnel test environment. Given the versatility of the RAM process to guide a wide spectrum of complex testing and modeling problems and the likely complex nature of vehicle designs in future UAM environments, this approach should be considered for future vehicle studies. Future work will further refine and extend the RAM process.

Acknowledgments

This work is supported by the NASA Transformational Tools and Technologies Project.

References

[1] Booze Allen Hamilton, Final Report Urban Air Mobility (UAM) Market Study https://ntrs.nasa.gov/archive/nasa/casi.ntrs.nasa.gov/20190001472.pdf .

[2] Crown Consulting, Inc., McKinsey & Company, Ascension Global, Georgia Tech, Urban Air Mobility (UAM) Market Study, https://www.nasa.gov/sites/default/files/atoms/files/uam-market-study-executive-summary-v2.pdf .

[3] Button, Keith, "For Vahana, A Study in Coping with Complexity," Aerospace America, June 2019.

[4] De Loach, R., "Applications of Modern Experiment Design to Wind Tunnel Testing at NASA Langley Research Center," AIAA 98-0713, *36th AIAA Aerospace Sciences Meeting and Exhibit*, Reno, NV, 1998.

[5] Morelli, E. A., and De Loach, R., "Ground Testing Results Using Modern Experiment Design and Multivariate Orthogonal Functions," AIAA 2003-0653, *41st AIAA Aerospace Sciences Meeting & Exhibit*, Reno, NV, 2003.

[6] Landman, Drew, Simpson, Jim, Vicroy, Dan, and Parker, Peter, "Response Surface Methods for Efficient Complex Aircraft Configuration Aerodynamic Characterization," *Journal of Aircraft*, Vol. 44, No. 4, July-August 2007. DOI: 10.2514/1.24810.

[7] Landman, Drew, Simpson, Jim, Mariani, Raffaello, Ortiz, Francisco, Britcher, Colin, "Hybrid Design for Aircraft Wind-Tunnel Testing Using Response Surface Methodologies," *Journal of Aircraft*, Vol. 44, No. 4, July-August 2007. DOI: 10.2514/1.25914.

[8] Landman, Drew, Simpson, Jim, Vicroy, Dan, and Parker, Peter, "Efficient Methods for Complex Aircraft Configuration Aerodynamic Characterization Using Response Surface Methodologies," *44th Aerospace Sciences Meeting and Exhibit*, January 2006. DOI: 10.2514/1.24810.

[9] Rothhaar, P., Murphy, P. C., Bacon, B. J., Grauer, J.; NASA Langley Distributed Propulsion VTOL Tilt Wing Aircraft Testing, Modeling, Simulation, Control, and Flight Test Development, AIAA AFM Conference, *AIAA Aviation 2014*, AIAA Paper No. 2014-2999.

[10] Busan, Ronald, Rothhaar, Paul, Croom, Mark, Murphy, Patrick C., Grafton, Sue, O'Neal, Anthony, "Enabling Advanced Wind-Tunnel Research Methods Using the NASA Langley 12-Foot Low Speed Tunnel," *AIAA Aviation and Aeronautics Forum and Exposition 2014*, AIAA Paper No. 2014-3000.
[11] Murphy, Patrick C. and Landman, Drew, "Experiment Design for Complex VTOL Aircraft with Distributed Propulsion and Tilt Wing," AIAA Atmospheric Flight Mechanics Conference, *AIAA SciTech 2015*, AIAA Paper No. 2015-0017.
[12] Murphy, Patrick C., Brandon, Jay, "Efficient Testing Combining Design of Experiment and Learn-to-Fly Strategies," *AIAA SciTech Forum*, Atmospheric Flight Mechanics Conference, AIAA 2017-0696, January, 2017. DOI: 10.2514/6.2017-0696.
[13] Simpson, James R. and Wisnowski, James W., "Streamlining Flight Test with the Design and Analysis of Experiments," *Journal of Aircraft*, Vol. 38, No. 6, November-December, 2001.
[14] Omran, Ashraf, Landman, Drew, Newman, Brett, "Global Stability and Control Derivative Modeling Using Design of Experiments," *AIAA Flight Mechanics Conference*, AIAA Paper No. 2009-5721, DOI: 10.2514/6.2009-5721.
[15] Brandon, Jay M., Morelli, Eugene A., "Nonlinear Aerodynamic Modeling From Flight Data Using Advanced Piloted Maneuvers and Fuzzy Logic," NASA/TM–2012-217778.
[16] Morelli, E. A., "Efficient Global Aerodynamic Modeling from Flight Data," *50th AIAA Aerospace Sciences Meeting*, AIAA Paper 2012-1050, January, 2012.
[17] Brandon, J. M. and Morelli, E. A., "Real-Time Global Nonlinear Aerodynamic Modeling from Flight Data," *Journal of Aircraft*, Vol. 53, No. 5, September-October, 2016, pp. 1261-1297.
[18] North, D. D., "Flight Testing of a Scale Urban Air Mobility Technology Testbed," *AIAA SciTech 2021 Forum*, Virtual Event, 2021. Presentation only.
[19] Williams, Brianne, Y., Landman, Drew, Flory, Isaac L., and Murphy, Patrick C., "The Effect of Systematic Error in Forced Oscillation Testing," *Aerospace Sciences Meeting*, AIAA Paper No. 2012-0768.
[20] Cummings, R.M. and Schütte, A., "Integrated Computational/Experimental Approach to Unmanned Combat Air Vehicle Stability and Control Estimation", *Journal of Aircraft*, Vol. 49, No. 6 (2012), pp. 1542-1557. doi: 10.2514/1.C03143.
[21] Ghoreyshi Mehdi, Cummings, Russell M., "Unsteady Aerodynamics Modeling for Aircraft Maneuvers: a New Approach Using Time-Dependent surrogate Modeling," 30th AIAA Applied Aerodynamics Conference, AIAA 2012-3327, June, 2012.
[22] Murphy, P.C., Klein, V., Frink, Neal T., and Vicroy, Dan D., "System Identification Applied to Dynamic CFD Simulation and Wind-Tunnel Data," *AIAA Atmospheric Flight Mechanics Conference*, AIAA 2011-6522, August, 2011.
[23] Murphy, Patrick C., Klein, Vladislav, Frink, Neal T.: Nonlinear Unsteady Aerodynamic Modeling Using Wind Tunnel and Computational Data. Journal of Aircraft. Vol. 54: 659-683, No. 2, March-April 2017. DOI: 10.2514/1.C033881.
[24] Frink, Neal T., Murphy, Patrick C., Atkins, Harold L., Viken, Sally A., Petrilli, Justin L.: Computational Aerodynamic Modeling Tools for Aircraft Loss-of-Control. *Journal of Guidance, Control, and Dynamics*. Vol. 40: 789-803, No. 4, April 2017. DOI: 10.2514/1 G001736.
[25] Derlaga, J. M., Jackson, C. W., and Buning, P. G., "Recent Progress in OVERFLOW Convergence Improvements," AIAA Paper 2020-1045, Jan. 2020.
[26] Buning, P. G., and Pulliam, T. H., "Near-Body Grid Adaption for Overset Grids," AIAA Paper 2016-3326, June 2016.
[27] Buning, P.G., Gomez, R. J., and Scallion, W. I., "CFD Approaches for Simulation of Wing-Body Stage Separation," AIAA-2004-4838, Aug. 2004.
[28] Geuther, S. C., and Fei, X., "LA-8 Computational Analysis and Validation Studies Using FlightStream," *AIAA SciTech 2021 Forum*, Virtual Event, 2021. To be published.
[29] North, D. D., Howland, G., and Busan, R. C. "Design and Fabrication of the LA-8 Distributed Electric Propulsion VTOL Testbed," *AIAA SciTech Forum*, January 2021 (to be published).
[30] Busan, R. C., Murphy, P. C., Hatke, D. B., and Simmons, B. M. "Wind Tunnel Testing Techniques for a Tandem Tilt- Wing, Distributed-Electric-Propulsion VTOL Aircraft," *AIAA SciTech Forum*, January 2021 (to be published).
[31] Geuther, S. C., North, D. D., and Busan, R. C., "Investigation of a Tandem Tilt-wing VTOL Aircraft in the NASA Langley 12-Foot Low-Speed Tunnel," NASA TM–2020–5003178, 2020.
[32] Simmons, B. M., and Murphy, P. C. "Wind Tunnel-Based Aerodynamic Model Identification for a Tilt-Wing, Distributed Electric Propulsion Aircraft," *AIAA SciTech 2021 Forum*, January 2021 (to be published).
[33] Simmons, B. M. "System Identification for Propellers at High Incidence Angles," AIAA SciTech Forum, January 2021 (to be published).
[34] Murphy, Patrick C., Hatke, David B., Aubuchon, Vanessa V., Weinstein, Rose, Busan, Ronald C., "Preliminary Steps in Developing Rapid Aero Modeling Technology," AIAA Atmospheric Flight Mechanics Conference, *AIAA SciTech 2020*, AIAA Paper No. 2020-0764.
[35] Murphy, Patrick C., Buning, Pieter G., Simmons, Benjamin M., "Rapid Aero Modeling for Urban Air Mobility Aircraft in Computational Tests," *AIAA SciTech 2021 Forum*, January 2021 (to be published).
[36] Silva, C., Johnson, W. Antcliff, Kevin R., Patterson, Michael D., "VTOL Urban Air Mobility Concept Vehicles for Technology Development," 2018 Aviation Technology, Integration, and Operations Conference, *AIAA Aviation Forum*, June 25-29, 2018, Atlanta, Georgia.
[37] Fisher, Ronald A., "The Design of Experiments," 9th ed., Macmillan. ISBN 0-02-844690-9, 1971 (1935).
[38] Klein, Vladislav and Morelli, Eugene A., "Aircraft System Identification: Theory and Practice," 1st edition, AIAA Inc., Reston, Virginia, 2006.
[39] Montgomery, Douglas, C., "Design and Analysis of Experiments," 8th ed., Wiley, 2013.

[40] Box, G. E. P. and Wilson, K. B., "On the experimental attainment of optimum conditions," *J. Roy. Statist. Soc.*, Ser. B Metho. Vol. 13, No. 1, pp. 1-45, 1951.
[41] De Loach, Richard, "Assessment of Response Surface Models Using Independent Confirmation Point Analysis," AIAA 2010-741, *48th AIAA Aerospace Sciences Meeting and Exhibit*, Orlando, FL, 2010.
[42] Ventura Diaz, P., and Yoon, S., "High-Fidelity Computational Aerodynamics of Multi-Rotor Unmanned Aerial Vehicles," AIAA Paper 2018-1266, Jan. 2018.
[43] Jia, Z., and Lee, S., "Acoustic Analysis of a Quadrotor eVTOL Design via High Fidelity Simulations," AIAA Paper 2019-2613, May 2019.
[44] VSPAero ref. Sandoz, Bryan, Vivek Ahuja, and Roy J. Hartfield. "Longitudinal Aerodynamic Characteristics of a V/STOL Tilt-wing Four-propeller Transport Model using a Surface Vorticity Flow Solver." *2018 AIAA Aerospace Sciences Meeting.* 2018. DOI:10.2514/6.2018-2070. http://openvsp.org/
[45] NDARC ref. Johnson, Wayne R., "NDARC NASA Design and Analysis of Rotorcraft Validation and Demonstration," NASA/TP-2015-218751, https://ntrs.nasa.gov/search.jsp?R=20110002948 2020-05-28T21:05:53+00:00Z.
[46] CAMRAD II Johnson, W. R. "CAMRAD II References," retrieved from http://johnson-aeronautics.com/documents/CAMRADreferences.pdf, Palo Alto, CA, 2018. https://software.nasa.gov/software/ARC-18184-1.
[47] Chaffin, M. S., & Berry, J. D., "Helicopter Fuselage Aerodynamics Under a Rotor by Navier-Stokes Simulation," *Journal of the American Helicopter Society*, Vol. 42, No. 3, pp. 235-243, 1997.
[48] Natoli, C., Burke, S., "Computer Experiments: Space Filling Design and Gaussian Process Modeling," STAT COE-Report-7-2018, Scientific Test and Analysis Techniques, Center of Excellence, www.afit.edu/STAT, Wright-Patterson AFB, OH.
[49] Weinstein, R., and Hubbard, J. E., "Global Aerodynamic Modeling using Automated Local Model Networks in Real Time," AIAA Atmospheric Flight Mechanics Conference, *AIAA SciTech Forum*, January 2020 (to be published).
[50] Cook, J. W., and Hauser, J., "A Strip Theory Approach to Dynamic Modeling of eVTOL Aircraft," *AIAA SciTech Forum*, January 2021. (to be published).